JETIR.ORG ISSN: 2349-5162 | ESTD Year : 2014 | Monthly Issue
JOURNAL OF EMERGING TECHNOLOGIES AND INNOVATIVE RESEARCH (JETIR)
An International Scholarly Open Access, Peer-reviewed, Refereed Journal

Intelligent Fault Detection and Mutually Exclusive Classification in Inverter-Dominated Power Grids Using sequence- Domain Artificial Neural Network

[1]Dayanada B S, [2]Maheshan C M

[1]Post Graduate Research Scholar, [2]Associate Professor
Dept. of EEE, UVCE,
Bengaluru, INDIA

Abstract : Rapid and selective fault identification is essential to safeguarding the operational stability of contemporary power distribution networks and microgrids, particularly those with high penetration of inverter-interfaced distributed generation (IIDG). Unlike synchronous machines, power-electronic inverters restrict fault current contributions to safeguard semiconductor switches, rendering traditional overcurrent protection schemes ineffective under low-fault-current regimes. To overcome this challenge, this paper develops a MATLAB/Simulink-based intelligent protection architecture that integrates symmetrical-component feature extraction with a multi-output Artificial Neural Network (ANN) and a decoupled deterministic post-processing logic layer. Three-phase root-mean-square (RMS) voltages, three-phase RMS currents, and zero-sequence voltage and current magnitudes are extracted at the monitoring bus to form a compact, noise-resilient feature vector. Trained on a balanced dataset of 2,000 operating instances spanning normal operation and eleven distinct shunt fault topologies—single line-to-ground (AG, BG, CG), double line-to-ground (ABG, BCG, ACG), line-to-line (AB, BC, CA), and symmetrical three-phase (ABC, ABCG) faults—the network achieves a test mean squared error (MSE) of 0.0284 and a regression correlation coefficient (R) of 0.9147. Furthermore, a combinational relational-AND decision circuit enforces strict mutual exclusivity among output channels while isolating diagnostic inference from physical fault injection. Dynamic time-domain simulations verify sub-cycle fault detection and zero cross-channel false tripping across asymmetrical and symmetrical disturbances.

IndexTerms **-** ***Artificial neural networks (ANN), fault classification, inverter-interfaced distributed generation (IIDG), microgrid protection, power system diagnostics, symmetrical sequence components*****.**

I. INTRODUCTION

Modern electrical power networks are undergoing a structural shift from centralized, synchronous-generator-dominated transmission topologies toward decentralized distribution grids and microgrids enriched with renewable energy sources. Because solar photovoltaic arrays, wind energy conversion systems, and battery energy storage units interface with the utility grid through power-electronic inverters, system fault behavior differs fundamentally from that of conventional radial networks [1], [4]. Specifically, inverter control loops actively limit output fault currents to roughly 1.1 to 2.0 per unit to protect power semiconductor devices from thermal damage. Consequently, conventional overcurrent relays and impedance-based protection schemes—which depend on high fault-current magnitudes and predictable unidirectional power flow—frequently suffer from delayed tripping, blind zones, or miscoordination during both grid-connected and islanded operating modes [3], [7].

To address these protection bottlenecks, data-driven fault detection and diagnosis (FDD) methodologies have attracted sustained research attention across smart grid and microgrid domains [2], [5], [9]. A substantial body of literature pairs time-frequency signal transforms with machine learning classifiers to capture transient fault signatures. For instance, discrete wavelet transform (DWT) decompositions combined with deep neural networks (DNNs) and adaptive neuro-fuzzy inference systems (ANFIS) have demonstrated strong classification accuracy in multi-area hybrid microgrids and multi-bus networks by isolating high-frequency transient energy at the point of common coupling [1], [8]. Similarly, hybrid frameworks integrating the S-Transform with particle filtering and neural classifiers have been explored to estimate fault direction and location under attenuated fault currents [4]. In direct-current (DC) and alternating-current (AC) microgrid architectures, comparative evaluations of artificial neural networks (ANNs), support vector machines (SVMs), decision trees (DTs), and k-nearest neighbors (kNNs) confirm that neural architectures offer superior generalization across fluctuating fault impedances and bidirectional converter power flows [3], [7], [10].

Despite these advances, several practical barriers hinder the deployment of complex deep-learning protection pipelines in real-time digital relays. Multi-stage time-frequency transforms and deep convolutional or recurrent architectures often impose heavy computational overhead, sensitivity to high-frequency measurement noise, and stringent training data requirements [6], [10]. Moreover, standalone neural network classifiers produce continuous probability or confidence vectors rather than crisp binary trip signals; without rigorous post-processing, overlapping confidence levels during transient inception can trigger simultaneous false alarms across multiple fault channels.

Motivated by the need for a computationally lightweight yet highly selective protection scheme, this paper presents a complete Simulink-based fault detection and classification framework built around steady-state and quasi-transient symmetrical-component features paired with a multi-output function-fitting ANN and a deterministic logic decoder. The primary contributions of this work are summarized as follows:

- **Compact Sequence-Domain Feature Representation:** Instead of computationally expensive multi-level wavelet decompositions, the proposed method utilizes three-phase root-mean-square (RMS) voltages and currents augmented by zero-sequence voltage and current components, providing immediate sensitivity to ground-involved asymmetrical disturbances.
- **Comprehensive Multi-Class Fault Coverage:** The neural classifier is trained and validated across 2,000 simulated operating records encompassing healthy grid states and all eleven standard shunt fault categories (AG, BG, CG, ABG, BCG, ACG, AB, BC, CA, ABC, and ABCG).
- **Mutually Exclusive Deterministic Logic Subsystem:** A dedicated combinational network of relational comparators and logical AND/OR gates decodes raw ANN confidence outputs into strictly mutually exclusive binary fault indicators, eliminating cross-channel false triggering during transient transitions.
- **Decoupled Simulation Architecture:** Diagnostic inference is structurally isolated from the physical fault-injection blocks within MATLAB/Simulink, guaranteeing numerical stability and preserving physical waveform fidelity.

The remainder of this paper is organized as follows. Section II details the power system modeling, symmetrical-component feature extraction, neural network training configuration, and deterministic classification logic. Section III describes the end-to-end operational workflow and dataset curation pipeline. Section IV presents quantitative training metrics and dynamic time-domain simulation results across representative fault scenarios. Finally, Section V concludes the study and outlines hardware-in-the-loop deployment pathways.

II. METHODOLOGY AND SYSTEM ARCHITECTURE

A. Power System Modeling and Signal Acquisition

To replicate realistic fault transients in a grid-connected distribution environment, a three-phase power system testbed is constructed in MATLAB/Simulink. The network comprises equivalent three-phase utility source feeders, step-down power transformers, distributed transmission/distribution line sections, programmable three-phase fault injection blocks, RMS measurement transducers, and symmetrical sequence analyzers. Under normal balanced operating conditions, three-phase voltages (Va, Vb, Vc) and line currents (Ia, Ib, Ic) maintain nominal magnitudes with 120° phase displacement. When a shunt disturbance occurs along the line, rapid voltage sags, current surges, and phase unbalances propagate toward the relaying point. To ensure consistent input scaling and robustness against switching harmonics, continuous instantaneous waveforms sampled at the relaying bus are converted into cycle-by-cycle RMS quantities. Because single-phase-to-ground and double-phase-to-ground faults inherently introduce zero-sequence unbalance that is absent in balanced three-phase and ungrounded line-to-line faults, Fortescue's symmetrical component transformation is applied to extract the zero-sequence voltage (V0) and zero-sequence current (I0) magnitudes:

$$V_0 = (1/3) \cdot (V_a + V_b + V_c), \quad I_0 = (1/3) \cdot (I_a + I_b + I_c) \tag{1}$$

Combining the six phase-domain RMS measurements with the two zero-sequence magnitudes yields an eight-dimensional input feature vector $x \in \mathbb{R}^8$ at each sampling instant:

$$x = [\, V_a,rms,\ V_b,rms,\ V_c,rms,\ I_a,rms,\ I_b,rms,\ I_c,rms,\ |V_0|,\ |I_0|\,]^T \tag{2}$$

All features are normalized prior to neural network ingestion so that voltage and current quantities contribute proportionally during gradient-based weight optimization, preventing high-magnitude current variations from dominating voltage-sag signatures.

B. Multi-Output Artificial Neural Network Architecture

Fault classification is formulated as a supervised multi-output pattern-recognition and function-fitting task. A feed-forward multi-layer perceptron (MLP) trained via scaled conjugate gradient / Levenberg-Marquardt backpropagation maps the normalized eight-element feature vector x to an eleven-element continuous confidence vector $y = [y_1, y_2, ..., y_{11}]^T$, where each output node corresponds to one of the eleven target shunt fault classes: single line-to-ground (AG, BG, CG), double line-to-ground (ABG, BCG, ACG), line-to-line (AB, BC, CA), and three-phase symmetrical faults (ABC, ABCG).

Within the Simulink environment, two coordinated function-fitting neural network blocks process the conditioned RMS and sequence inputs in parallel to evaluate fault presence and multi-class confidence scores. During supervised training, target vectors are encoded using binary one-hot representations (1.0 for the active fault state and 0.0 for all inactive states). The network minimizes the Mean Squared Error (MSE) objective function across N training observations:

$$MSE = (1/(N \cdot K)) \cdot \sum_{i=1}^{N} \sum_{k=1}^{K} (t_{i,k} - y_{i,k})^2 \tag{3}$$

where K = 11 denotes the number of output fault classes, $t_{i,k}$ represents the ground-truth target label, and $y_{i,k}$ is the predicted neural network output for the i-th sample.

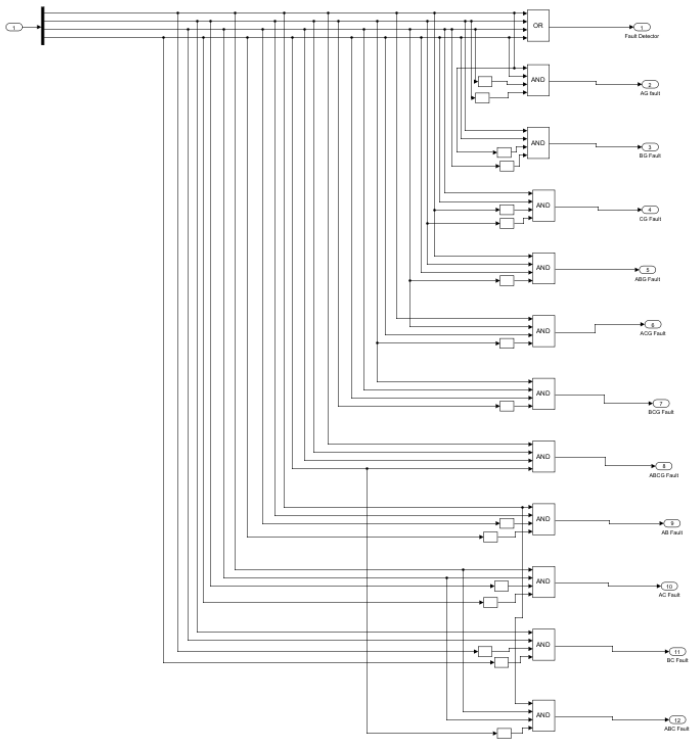

Fig. 1: *Validation performance trajectory of the artificial neural network across 94 training epochs, achieving minimum validation MSE of 0.031781 at epoch 88.*

C. Deterministic Post-ANN Fault Classification Logic Subsystem

Because an ANN trained with continuous activation functions generates real-valued outputs in the range [0, 1], raw network predictions can exhibit minor non-zero ripples on non-faulted channels during the initial half-cycle after fault inception. Relying directly on unconditioned threshold comparisons risks simultaneous assertion of multiple fault flags (for example, momentarily confusing an ABG fault with an AG or AB fault). To guarantee crisp, unambiguous relay decisions, a deterministic combinational logic subsystem is cascaded after the ANN output layer.

First, each neural output channel y_k is evaluated against a calibrated decision threshold τ via relational comparators to produce intermediate binary logic states. Second, a structured network of multi-input logical AND gates and logical NOT inverters enforces mutual exclusivity across all eleven fault categories, while a master logical OR gate aggregates all class outputs to generate a unified global Fault Detector trip flag (F_det):

$$F_det = V_{k=1}^{11} D_k, \quad D_k = (y_k > \tau) \wedge \wedge_{j \neq k} \neg(y_j > y_k) \tag{4}$$

As illustrated in Fig. 2, this combinational logic circuit ensures that at most one fault class indicator D_k can transition to a logical high state (1) at any time step, while all non-faulted channels remain strictly clamped at zero (0). Crucially, the entire diagnostic and logic subsystem is structurally decoupled from the physical fault-injection switches in Simulink; output signals serve exclusively for monitoring and relay actuation without feeding back into the electrical network equations, thereby preserving numerical convergence and physical model integrity.

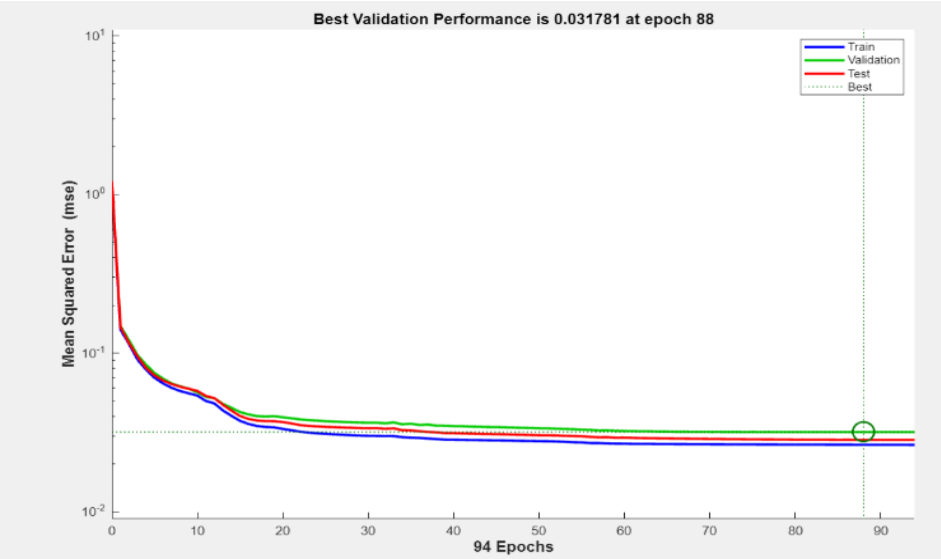

Fig. 2: *Simulink implementation of the deterministic post-ANN fault classification logic subsystem utilizing relational comparators, inverters, and multi-input AND/OR gates.*

III. PROPOSED OPERATIONAL WORKFLOW

Fig. 3 illustrates the redesigned end-to-end architecture of the proposed intelligent fault diagnosis framework, clearly delineating online Simulink signal acquisition, offline dataset engineering in Google Colaboratory, and real-time neural inference with deterministic relay logic.

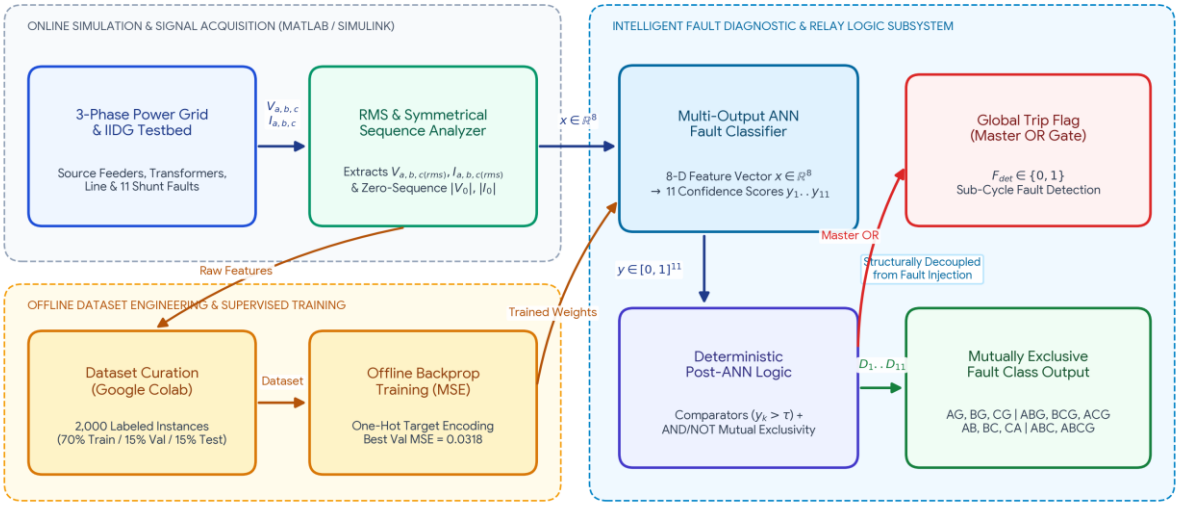

Fig. 3: *End-to-end architecture of the proposed sequence-domain ANN fault detection and classification workflow.*

The operational pipeline executes through four sequential stages:

Stage 1 — Multi-Scenario Fault Simulation: The three-phase power grid model is simulated across healthy steady-state conditions and all eleven shunt fault permutations. Fault inception times, fault resistances, and phase combinations are systematically varied to capture diverse transient and post-fault steady-state operating envelopes.

Stage 2 — Feature Conditioning and Dataset Curation: Measured three-phase voltages and currents are passed through RMS and zero-sequence extraction blocks. To streamline data preprocessing, class labeling, and stratified partitioning, Google Colaboratory is utilized as an auxiliary data-engineering environment to structure and export 2,000 labeled observations into standardized spreadsheet datasets for neural network training.

Stage 3 — Offline Training and Validation: The curated 2,000-sample dataset is partitioned into three disjoint subsets using a 70% / 15% / 15% split: 1,400 samples for network weight training, 300 samples for cross-validation and early-stopping regularization, and 300 unseen samples for independent generalization testing.

Stage 4 — Real-Time Simulink Deployment: Once convergence criteria are satisfied, the trained synaptic weights and biases are embedded directly into the Simulink function-fitting neural blocks and coupled with the deterministic logic subsystem for online time-domain fault classification.

IV. SIMULATION RESULTS AND DISCUSSION

A. Quantitative Training, Validation, and Testing Performance

The training convergence behavior of the proposed ANN is depicted in Fig. 1. Across 94 training epochs, the training, validation, and testing MSE curves decrease monotonically by nearly two orders of magnitude from an initial error above 10^0, stabilizing smoothly without divergence or overfitting. Early stopping triggers at epoch 94 after recording the best validation performance of MSE = 0.031781 at epoch 88. Table I summarizes the quantitative performance across all three dataset partitions.

TABLE I
QUANTITATIVE PERFORMANCE METRICS OF THE TRAINED ANN CLASSIFIER

Dataset Partition	Observations (N)	Mean Squared Error (MSE)	Regression Correlation (R)
Training Set (70%)	1,400	0.0264	0.9202
Validation Set (15%)	300	0.0318	0.9039
Testing Set (15%)	300	0.0284	0.9147

As reported in Table I, the close alignment between training MSE (0.0264), validation MSE (0.0318), and unseen testing MSE (0.0284)—paired with regression correlation coefficients exceeding 0.90 across all partitions (R = 0.9147 on the independent test set)—confirms strong out-of-sample generalization without memorization of training noise.

B. Dynamic Time-Domain Fault Detection and Selectivity Analysis

To evaluate transient detection speed and channel selectivity under live simulation conditions, time-domain fault injection tests were conducted over a 0.20 s simulation window with disturbances initiated at t = 0.10 s. Fig. 4 illustrates the high-resolution twelve-channel diagnostic scope response during a double line-to-ground (ABG) fault event.

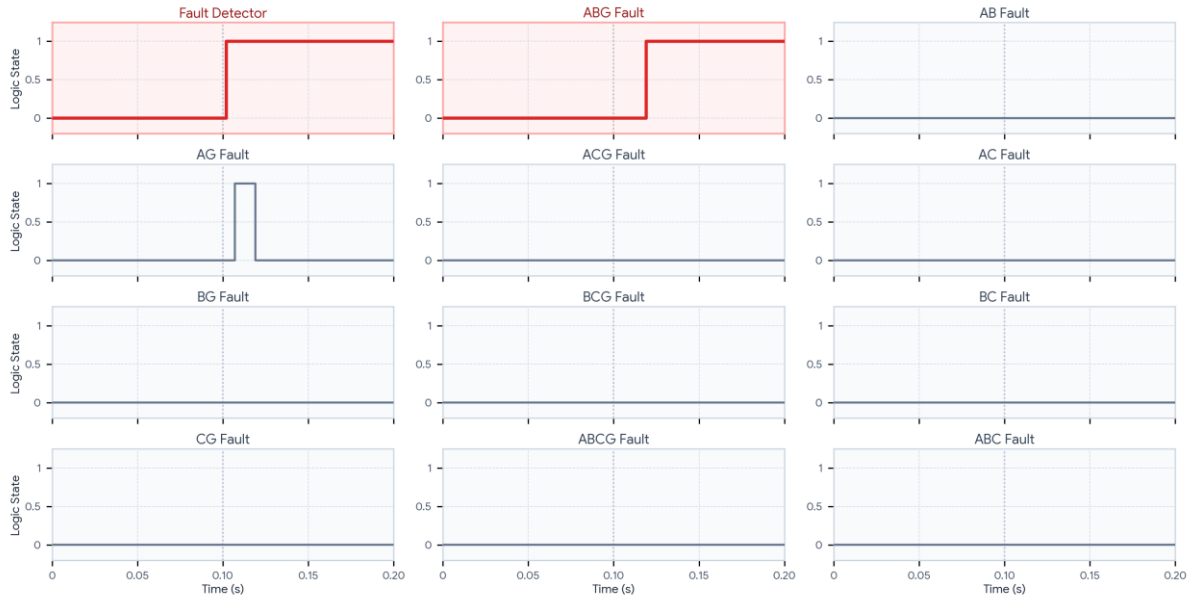

Fig. 4: *Dynamic twelve-channel diagnostic response during a double line-to-ground (ABG) fault initiated at t = 0.10 s, demonstrating rapid global Fault Detector assertion and post-transient isolation of the ABG output channel.*

As observed in Fig. 4, the master Fault Detector flag transitions immediately from 0 to 1 upon fault inception at t ≈ 0.102 s, confirming rapid anomaly recognition. During the initial sub-cycle RMS window transition (between t = 0.107 s and t = 0.119 s), the single-phase AG channel briefly registers a transient pulse as phase-A current rises ahead of phase-B stabilization; immediately thereafter, the deterministic post-ANN logic locks onto the true ABG fault class (logic 1) while resetting AG to 0 and holding all remaining nine channels (BG, CG, ACG, BCG, ABCG, AB, AC, BC, ABC) strictly at 0 for the remainder of the event.

Fig. 5 depicts the corresponding system response under a single line-to-ground (BG) fault disturbance initiated at t = 0.10 s. Immediately following fault inception, the global Fault Detector asserts a sustained high state, and the BG fault indicator rises cleanly to logic 1 without any transient or steady-state false triggering across the remaining ten fault channels.

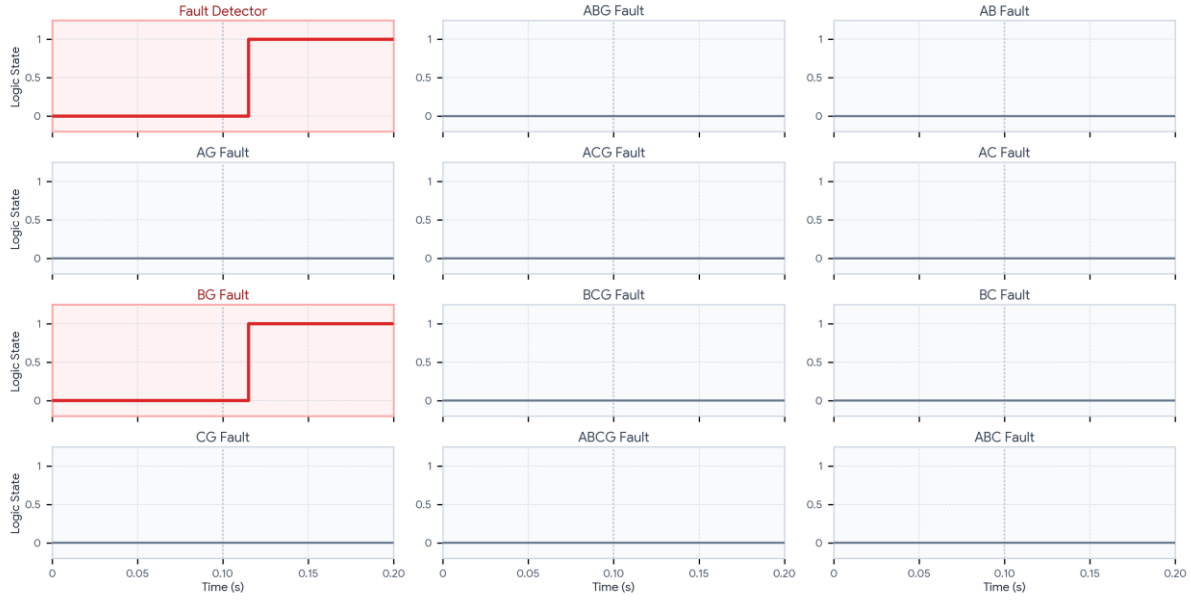

Fig. 5: *Dynamic twelve-channel diagnostic response during a single line-to-ground (BG) fault initiated at t = 0.10 s, confirming immediate detection and complete absence of cross-channel false triggering.*

Comparable selective responses were verified across the remaining single-phase (AG, CG), double-line-to-ground (ACG, BCG), line-to-line (AB, BC, CA), and symmetrical three-phase (ABC, ABCG) fault scenarios. Across all tested operating conditions, the combination of zero-sequence feature augmentation and relational-AND output decoding reliably distinguished grounded from ungrounded disturbances while maintaining strict mutual exclusivity.

V. CONCLUSION AND FUTURE SCOPE

This paper has presented an intelligent, computationally streamlined fault detection and classification scheme tailored for modern three-phase power grids and inverter-integrated microgrids. By pairing cycle-by-cycle RMS phase voltage and current measurements with zero-sequence voltage and current components, the proposed eight-feature input representation captures asymmetrical and symmetrical fault signatures without requiring heavy multi-resolution wavelet preprocessing. Trained across 2,000 simulated operating cases, the multi-output ANN achieved a test MSE of 0.0284 and a correlation coefficient of 0.9147. Furthermore, cascading a decoupled combinational logic subsystem after the ANN effectively enforced mutual exclusivity across all eleven shunt fault classes and eliminated steady-state false alarms.

Future research will focus on translating the trained neural weights and deterministic logic gates onto embedded hardware targets—specifically field-programmable gate arrays (FPGAs) and digital signal processors (DSPs)—for real-time hardware-in-the-loop (HIL) validation. Planned extensions also include incorporating fault-distance estimation and testing classifier resilience under high-impedance faults, current transformer saturation, and islanded microgrid mode transitions.

..

REFERENCES

[1] S. N. V. Bramareswara Rao, Y. V. Pavan Kumar, and M. Amir, "Fault detection and classification in hybrid energy-based multi-area grid-connected microgrid clusters using discrete wavelet transform with deep neural networks," Electrical Engineering, vol. 107, pp. 8481–8498, 2025, doi: 10.1007/s00202-024-02329-4.

[2] S. F. Nasim, S. Aziz, A. Qaiser, U.-e.-Kulsoom, and S. Ahmed, "Fault detection and fault diagnosis in power system using AI: A review," Sir Syed University Research Journal of Engineering & Technology, vol. 14, no. 1, 2024, doi: 10.33317/ssurj.598.

[3] G. Goyal, I. T. Salsabil, A. Kumar, M. Ukey, and V. P. S. Velumani, "AI-driven fault detection and diagnosis in smart grids for enhanced power system reliability," Journal of Information Systems Engineering and Management, vol. 10, no. 42s, 2025.

[4] Archana and S. K. Sharma, "An intelligent particle filter with neural network for fault location and classification in microgrid," Journal of Informatics Electrical and Electronics Engineering, vol. 6, no. 1, pp. 1–11, 2025.

[5] M. Ekanayake, "Artificial intelligence for fault detection and diagnosis in power distribution systems," Journal of Electrical & Electronic Systems, vol. 13, no. 5, 2024.

[6] Y. Zhao, T. Li, X. Zhang, and C. Zhang, "Artificial intelligence-based fault detection and diagnosis methods for building energy systems: Advantages, challenges and the future," Renewable and Sustainable Energy Reviews, vol. 109, pp. 398–422, 2019, doi: 10.1016/j.rser.2019.04.021.

[7] S. P. Tiwari, "Artificial neural network based algorithm for fault detection in a ring DC microgrid under diverse fault conditions," Distributed Generation & Alternative Energy Journal, vol. 38, no. 1, pp. 23–40, 2022, doi: 10.13052/dgaej2156-3306.3812.

[8] P. Ingole and A. V. Mohod, "Fault detection scheme of 5 bus by ANN and ANFIS," International Research Journal of Engineering and Technology (IRJET), vol. 9, no. 3, Mar. 2022.

[9] O. A. Omitaomu and H. Niu, "Artificial intelligence techniques in smart grid: A survey," Energies, vol. 13, no. 19, Art. no. 5199, 2020, doi: 10.3390/en13195199.

[10] S. R. Fahim, S. K. Sarker, M. R. I. Sheikh, S. M. Muyeen, and S. K. Das, "Microgrid fault detection and classification: Machine learning based approach, comparison, and reviews," Energies, vol. 13, no. 13, Art. no. 3460, 2020, doi: 10.3390/en13133460.